

First combined analysis of neutrino and antineutrino oscillations at T2K

K. Abe,⁴⁷ J. Amey,¹⁶ C. Andreopoulos,^{45,26} M. Antonova,²¹ S. Aoki,²³ A. Ariga,¹ D. Autiero,²⁸ S. Ban,²⁴ M. Barbi,³⁹ G.J. Barker,⁵⁵ G. Barr,³⁵ C. Barry,²⁶ P. Bartet-Friburg,³⁶ M. Batkiewicz,¹² V. Berardi,¹⁷ S. Berkman,^{3,51} S. Bhadra,⁶⁰ S. Bienstock,³⁶ A. Blondel,¹¹ S. Bolognesi,⁵ S. Bordini,¹⁴ S.B. Boyd,⁵⁵ D. Brailsford,²⁵ A. Bravar,¹¹ C. Bronner,²² M. Buizza Avanzini,⁹ R.G. Calland,²² T. Campbell,⁷ S. Cao,¹³ S.L. Cartwright,⁴³ M.G. Catanesi,¹⁷ A. Cervera,¹⁵ C. Checchia,¹⁹ D. Cherdack,⁷ N. Chikuma,⁴⁶ G. Christodoulou,²⁶ A. Clifton,⁷ J. Coleman,²⁶ G. Collazuol,¹⁹ D. Coplowe,³⁵ A. Cudd,²⁹ A. Dabrowska,¹² G. De Rosa,¹⁸ T. Dealtry,²⁵ P.F. Denner,⁵⁵ S.R. Dennis,²⁶ C. Densham,⁴⁵ D. Dewhurst,³⁵ F. Di Lodovico,³⁸ S. Di Luise,¹⁰ S. Dolan,³⁵ O. Drapier,⁹ K.E. Duffy,³⁵ J. Dumarchez,³⁶ M. Dziewiecki,⁵⁴ S. Emery-Schrenk,⁵ A. Ereditato,¹ T. Feusels,^{3,51} A.J. Finch,²⁵ G.A. Fiorentini,⁶⁰ M. Friend,^{13,*} Y. Fujii,^{13,*} D. Fukuda,³³ Y. Fukuda,³⁰ V. Galymov,²⁸ A. Garcia,¹⁴ C. Giganti,³⁶ F. Gizzarelli,⁵ T. Golan,⁵⁸ M. Gonin,⁹ D.R. Hadley,⁵⁵ L. Haegel,¹¹ M.D. Haigh,⁵⁵ D. Hansen,³⁷ J. Harada,³⁴ M. Hartz,^{22,51} T. Hasegawa,^{13,*} N.C. Hastings,³⁹ T. Hayashino,²⁴ Y. Hayato,^{47,22} R.L. Helmer,⁵¹ A. Hillairet,⁵² T. Hiraki,²⁴ A. Hiramoto,²⁴ S. Hirota,²⁴ M. Hogan,⁷ J. Holeczek,⁴⁴ F. Hosomi,⁴⁶ K. Huang,²⁴ A.K. Ichikawa,²⁴ M. Ikeda,⁴⁷ J. Imber,⁹ J. Insler,²⁷ R.A. Intonti,¹⁷ T. Ishida,^{13,*} T. Ishii,^{13,*} E. Iwai,¹³ K. Iwamoto,⁴⁰ A. Izmaylov,^{15,21} B. Jamieson,⁵⁷ M. Jiang,²⁴ S. Johnson,⁶ P. Jonsson,¹⁶ C.K. Jung,^{32,†} M. Kabirnezhad,³¹ A.C. Kaboth,^{41,45} T. Kajita,^{48,†} H. Kakuno,⁴⁹ J. Kameda,⁴⁷ D. Karlen,^{52,51} T. Katori,³⁸ E. Kearns,^{2,22,†} M. Khabibullin,²¹ A. Khotjantsev,²¹ H. Kim,³⁴ J. Kim,^{3,51} S. King,³⁸ J. Kisiel,⁴⁴ A. Knight,⁵⁵ A. Knox,²⁵ T. Kobayashi,^{13,*} L. Koch,⁴² T. Koga,⁴⁶ A. Konaka,⁵¹ K. Kondo,²⁴ L.L. Kormos,²⁵ A. Korzenev,¹¹ Y. Koshio,^{33,†} K. Kowalik,³¹ W. Kropp,⁴ Y. Kudenko,^{21,‡} R. Kurjata,⁵⁴ T. Kutter,²⁷ J. Lagoda,³¹ I. Lamont,²⁵ M. Lamoureux,⁵ E. Larkin,⁵⁵ P. Lasorak,³⁸ M. Laveder,¹⁹ M. Lawe,²⁵ M. Licciardi,⁹ T. Lindner,⁵¹ Z.J. Liptak,⁶ R.P. Litchfield,¹⁶ X. Li,³² A. Longhin,¹⁹ J.P. Lopez,⁶ T. Lou,⁴⁶ L. Ludovici,²⁰ X. Lu,³⁵ L. Magaletti,¹⁷ K. Mahn,²⁹ M. Malek,⁴³ S. Manly,⁴⁰ A.D. Marino,⁶ J.F. Martin,⁵⁰ P. Martins,³⁸ S. Martynenko,³² T. Maruyama,^{13,*} V. Matveev,²¹ K. Mavrokoridis,²⁶ W.Y. Ma,¹⁶ E. Mazzucato,⁵ M. McCarthy,⁶⁰ N. McCauley,²⁶ K.S. McFarland,⁴⁰ C. McGrew,³² A. Mefodiev,²¹ C. Metelko,²⁶ M. Mezzetto,¹⁹ P. Mijakowski,³¹ A. Minamino,⁵⁹ O. Mineev,²¹ S. Mine,⁴ A. Missert,⁶ M. Miura,^{47,†} S. Moriyama,^{47,†} Th.A. Mueller,⁹ J. Myslik,⁵² T. Nakadaira,^{13,*} M. Nakahata,^{47,22} K.G. Nakamura,²⁴ K. Nakamura,^{22,13,*} K.D. Nakamura,²⁴ Y. Nakanishi,²⁴ S. Nakayama,^{47,†} T. Nakaya,^{24,22} K. Nakayoshi,^{13,*} C. Nantais,⁵⁰ C. Nielsen,³ M. Nirkko,¹ K. Nishikawa,^{13,*} Y. Nishimura,⁴⁸ P. Novella,¹⁵ J. Nowak,²⁵ H.M. O’Keeffe,²⁵ K. Okumura,^{48,22} T. Okusawa,³⁴ W. Oryszczak,⁵³ S.M. Oser,^{3,51} T. Ovsyannikova,²¹ R.A. Owen,³⁸ Y. Oyama,^{13,*} V. Palladino,¹⁸ J.L. Palomino,³² V. Paolone,³⁷ N.D. Patel,²⁴ P. Paudyal,²⁶ M. Pavin,³⁶ D. Payne,²⁶ J.D. Perkin,⁴³ Y. Petrov,^{3,51} L. Pickard,⁴³ L. Pickering,¹⁶ E.S. Pinzon Guerra,⁶⁰ C. Pistillo,¹ B. Popov,^{36,§} M. Posiadala-Zezula,⁵³ J.-M. Poutissou,⁵¹ R. Poutissou,⁵¹ P. Przewlocki,³¹ B. Quilain,²⁴ T. Radermacher,⁴² E. Radicioni,¹⁷ P.N. Ratoff,²⁵ M. Ravonel,¹¹ M.A. Rayner,¹¹ A. Redij,¹ E. Reinherz-Aronis,⁷ C. Riccio,¹⁸ P.A. Rodrigues,⁴⁰ E. Rondio,³¹ B. Rossi,¹⁸ S. Roth,⁴² A. Rubbia,¹⁰ A. Rychter,⁵⁴ K. Sakashita,^{13,*} F. Sánchez,¹⁴ E. Scantamburlo,¹¹ K. Scholberg,^{8,†} J. Schwehr,⁷ M. Scott,⁵¹ Y. Seiya,³⁴ T. Sekiguchi,^{13,*} H. Sekiya,^{47,22,†} D. Sgalaberna,¹¹ R. Shah,^{45,35} A. Shaikhiev,²¹ F. Shaker,⁵⁷ D. Shaw,²⁵ M. Shiozawa,^{47,22} T. Shirahige,³³ S. Short,³⁸ M. Smy,⁴ J.T. Sobczyk,⁵⁸ H. Sobel,^{4,22} M. Sorel,¹⁵ L. Southwell,²⁵ J. Steinmann,⁴² T. Stewart,⁴⁵ P. Stowell,⁴³ Y. Suda,⁴⁶ S. Suvorov,²¹ A. Suzuki,²³ S.Y. Suzuki,^{13,*} Y. Suzuki,²² R. Tacik,^{39,51} M. Tada,^{13,*} A. Takeda,⁴⁷ Y. Takeuchi,^{23,22} H.K. Tanaka,^{47,†} H.A. Tanaka,^{50,51,¶} D. Terhorst,⁴² R. Terri,³⁸ T. Thakore,²⁷ L.F. Thompson,⁴³ S. Tobayama,^{3,51} W. Toki,⁷ T. Tomura,⁴⁷ C. Touramanis,²⁶ T. Tsukamoto,^{13,*} M. Tzanov,²⁷ Y. Uchida,¹⁶ M. Vagins,^{22,4} Z. Vallari,³² G. Vasseur,⁵ T. Vladislavljjevic,^{35,22} T. Wachala,¹² C.W. Walter,^{8,†} D. Wark,^{45,35} M.O. Wascko,^{16,13} A. Weber,^{45,35} R. Wendell,^{24,†} R.J. Wilkes,⁵⁶ M.J. Wilking,³² C. Wilkinson,¹ J.R. Wilson,³⁸ R.J. Wilson,⁷ C. Wret,¹⁶ Y. Yamada,^{13,*} K. Yamamoto,³⁴ M. Yamamoto,²⁴ C. Yanagisawa,^{32,**} T. Yano,²³ S. Yen,⁵¹ N. Yershov,²¹ M. Yokoyama,^{46,†} K. Yoshida,²⁴ T. Yuan,⁶ M. Yu,⁶⁰ A. Zalewska,¹² J. Zalipska,³¹ L. Zambelli,^{13,*} K. Zaremba,⁵⁴ M. Ziembicki,⁵⁴ E.D. Zimmerman,⁶ M. Zito,⁵ and J. Żmuda⁵⁸

(The T2K Collaboration)

¹University of Bern, Albert Einstein Center for Fundamental Physics,
Laboratory for High Energy Physics (LHEP), Bern, Switzerland

²Boston University, Department of Physics, Boston, Massachusetts, U.S.A.

³University of British Columbia, Department of Physics and Astronomy, Vancouver, British Columbia, Canada

⁴University of California, Irvine, Department of Physics and Astronomy, Irvine, California, U.S.A.

⁵IRFU, CEA Saclay, Gif-sur-Yvette, France

⁶University of Colorado at Boulder, Department of Physics, Boulder, Colorado, U.S.A.

- ⁷Colorado State University, Department of Physics, Fort Collins, Colorado, U.S.A.
⁸Duke University, Department of Physics, Durham, North Carolina, U.S.A.
⁹Ecole Polytechnique, IN2P3-CNRS, Laboratoire Leprince-Ringuet, Palaiseau, France
¹⁰ETH Zurich, Institute for Particle Physics, Zurich, Switzerland
¹¹University of Geneva, Section de Physique, DPNC, Geneva, Switzerland
¹²H. Niewodniczanski Institute of Nuclear Physics PAN, Cracow, Poland
¹³High Energy Accelerator Research Organization (KEK), Tsukuba, Ibaraki, Japan
¹⁴Institut de Fisica d'Altes Energies (IFAE), The Barcelona Institute of Science and Technology, Campus UAB, Bellaterra (Barcelona) Spain
¹⁵IFIC (CSIC & University of Valencia), Valencia, Spain
¹⁶Imperial College London, Department of Physics, London, United Kingdom
¹⁷INFN Sezione di Bari and Università e Politecnico di Bari, Dipartimento Interuniversitario di Fisica, Bari, Italy
¹⁸INFN Sezione di Napoli and Università di Napoli, Dipartimento di Fisica, Napoli, Italy
¹⁹INFN Sezione di Padova and Università di Padova, Dipartimento di Fisica, Padova, Italy
²⁰INFN Sezione di Roma and Università di Roma "La Sapienza", Roma, Italy
²¹Institute for Nuclear Research of the Russian Academy of Sciences, Moscow, Russia
²²Kavli Institute for the Physics and Mathematics of the Universe (WPI), The University of Tokyo Institutes for Advanced Study, University of Tokyo, Kashiwa, Chiba, Japan
²³Kobe University, Kobe, Japan
²⁴Kyoto University, Department of Physics, Kyoto, Japan
²⁵Lancaster University, Physics Department, Lancaster, United Kingdom
²⁶University of Liverpool, Department of Physics, Liverpool, United Kingdom
²⁷Louisiana State University, Department of Physics and Astronomy, Baton Rouge, Louisiana, U.S.A.
²⁸Université de Lyon, Université Claude Bernard Lyon 1, IPN Lyon (IN2P3), Villeurbanne, France
²⁹Michigan State University, Department of Physics and Astronomy, East Lansing, Michigan, U.S.A.
³⁰Miyagi University of Education, Department of Physics, Sendai, Japan
³¹National Centre for Nuclear Research, Warsaw, Poland
³²State University of New York at Stony Brook, Department of Physics and Astronomy, Stony Brook, New York, U.S.A.
³³Okayama University, Department of Physics, Okayama, Japan
³⁴Osaka City University, Department of Physics, Osaka, Japan
³⁵Oxford University, Department of Physics, Oxford, United Kingdom
³⁶UPMC, Université Paris Diderot, CNRS/IN2P3, Laboratoire de Physique Nucléaire et de Hautes Energies (LPNHE), Paris, France
³⁷University of Pittsburgh, Department of Physics and Astronomy, Pittsburgh, Pennsylvania, U.S.A.
³⁸Queen Mary University of London, School of Physics and Astronomy, London, United Kingdom
³⁹University of Regina, Department of Physics, Regina, Saskatchewan, Canada
⁴⁰University of Rochester, Department of Physics and Astronomy, Rochester, New York, U.S.A.
⁴¹Royal Holloway University of London, Department of Physics, Egham, Surrey, United Kingdom
⁴²RWTH Aachen University, III. Physikalisches Institut, Aachen, Germany
⁴³University of Sheffield, Department of Physics and Astronomy, Sheffield, United Kingdom
⁴⁴University of Silesia, Institute of Physics, Katowice, Poland
⁴⁵STFC, Rutherford Appleton Laboratory, Harwell Oxford, and Daresbury Laboratory, Warrington, United Kingdom
⁴⁶University of Tokyo, Department of Physics, Tokyo, Japan
⁴⁷University of Tokyo, Institute for Cosmic Ray Research, Kamioka Observatory, Kamioka, Japan
⁴⁸University of Tokyo, Institute for Cosmic Ray Research, Research Center for Cosmic Neutrinos, Kashiwa, Japan
⁴⁹Tokyo Metropolitan University, Department of Physics, Tokyo, Japan
⁵⁰University of Toronto, Department of Physics, Toronto, Ontario, Canada
⁵¹TRIUMF, Vancouver, British Columbia, Canada
⁵²University of Victoria, Department of Physics and Astronomy, Victoria, British Columbia, Canada
⁵³University of Warsaw, Faculty of Physics, Warsaw, Poland
⁵⁴Warsaw University of Technology, Institute of Radioelectronics, Warsaw, Poland
⁵⁵University of Warwick, Department of Physics, Coventry, United Kingdom
⁵⁶University of Washington, Department of Physics, Seattle, Washington, U.S.A.
⁵⁷University of Winnipeg, Department of Physics, Winnipeg, Manitoba, Canada
⁵⁸Wroclaw University, Faculty of Physics and Astronomy, Wroclaw, Poland
⁵⁹Yokohama National University, Faculty of Engineering, Yokohama, Japan
⁶⁰York University, Department of Physics and Astronomy, Toronto, Ontario, Canada

(Dated: March 3, 2022)

T2K reports its first results in the search for CP violation in neutrino oscillations using appearance and disappearance channels for neutrino- and antineutrino-mode beam. The data include all runs from Jan 2010 to May 2016 and comprise 7.482×10^{20} protons on target in neutrino mode, which yielded in the far detector 32 e-like and 135 μ -like events, and 7.471×10^{20} protons on target in antineutrino mode which yielded 4 e-like and 66 μ -like events. Reactor measurements of $\sin^2 2\theta_{13}$

have been used as an additional constraint. The one-dimensional confidence interval at 90% for δ_{CP} spans the range $(-3.13, -0.39)$ for normal mass ordering. The CP conservation hypothesis ($\delta_{CP} = 0, \pi$) is excluded at 90% C.L.

PACS numbers: 14.60.Pq, 14.60.Lm, 11.30.Er, 95.55.Vj

Introduction — A new source of CP violation beyond the CKM quark mixing matrix is necessary to explain observations of baryon asymmetry in the Universe. In the lepton sector the PMNS framework [1, 2] allows for CP violation. The first indication of non-zero θ_{13} [3] followed by its discovery [4–6] and then the discovery of $\nu_\mu \rightarrow \nu_e$ oscillation by T2K [7] have opened the possibility to look for CP violation in neutrino oscillation.

In this Letter we present the first joint fit of neutrino and antineutrino $\bar{\nu}_\mu \rightarrow \bar{\nu}_e$ and $\bar{\nu}_\mu \rightarrow \bar{\nu}_\mu$ oscillation at T2K. The mixing of neutrinos in the three-flavour framework is represented by the unitary PMNS matrix, parameterized by three mixing angles, θ_{12} , θ_{13} , and θ_{23} , and a CP-violating phase δ_{CP} [8]. The probability for $\bar{\nu}_\mu \rightarrow \bar{\nu}_e$ oscillation, as a function of neutrino propagation distance L and energy E , can be written:

$$\begin{aligned}
 P(\bar{\nu}_\mu \rightarrow \bar{\nu}_e) &\simeq \sin^2 \theta_{23} \sin^2 2\theta_{13} \sin^2 \frac{\Delta m_{31}^2 L}{4E} \\
 &\quad - \frac{^{(+)} \sin 2\theta_{12} \sin 2\theta_{23}}{2 \sin \theta_{13}} \sin \frac{\Delta m_{21}^2 L}{4E} \\
 &\quad \times \sin^2 2\theta_{13} \sin^2 \frac{\Delta m_{31}^2 L}{4E} \sin \delta_{CP} \\
 &\quad + (\text{CP-even, solar, matter effect terms}) \quad (1)
 \end{aligned}$$

where $\Delta m_{ij}^2 = m_i^2 - m_j^2$ represents the neutrino mass-squared difference between mass eigenstates i and j . The $\bar{\nu}_\mu \rightarrow \bar{\nu}_\mu$ survival probability is dominated by the parameters $\sin^2 \theta_{23}$ and Δm_{32}^2 , as given in [9]. Comparing electron neutrino and antineutrino appearance probabilities allows a direct measurement of CP violation at T2K. The asymmetry variable ($A_{CP} = P(\nu_\mu \rightarrow \nu_e) - P(\bar{\nu}_\mu \rightarrow \bar{\nu}_e) / (P(\nu_\mu \rightarrow \nu_e) + P(\bar{\nu}_\mu \rightarrow \bar{\nu}_e))$) and the ν_μ ($\bar{\nu}_\mu$) component of the expected T2K flux without oscillations are shown in Fig. 1. At the flux peak energy, A_{CP} can be as large as 0.4, including a contribution of around 0.1 due to matter effects.

The T2K Experiment — The T2K experiment [10] uses a 30 GeV proton beam from the J-PARC accelerator facility to produce a muon (anti)neutrino beam. The proton beam strikes a graphite target to produce charged pions and kaons, which are focused by three magnetic horns. Depending on the polarity of the horn current, either positively- or negatively-charged mesons are focused, resulting in a beam largely composed of muon neutrinos or antineutrinos. A 96-m decay volume lies downstream of the magnetic horns, followed by the beam dump and muon monitor [11]. The neutrino beam is measured by detectors placed on axis and off axis at 2.5° relative to the beam direction. The off-axis neutrino energy spectrum

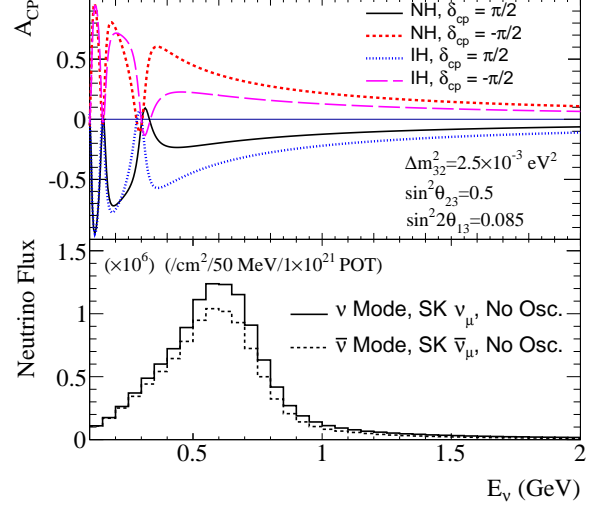


FIG. 1. The leptonic CP asymmetry, $A_{CP} = [P(\nu_\mu \rightarrow \nu_e) - P(\bar{\nu}_\mu \rightarrow \bar{\nu}_e)] / [P(\nu_\mu \rightarrow \nu_e) + P(\bar{\nu}_\mu \rightarrow \bar{\nu}_e)]$, as a function of energy for maximal CP-violation hypotheses (top) and the ν_μ ($\bar{\nu}_\mu$) component of the unoscillated (anti)neutrino flux in neutrino and antineutrino modes (bottom).

peaks at 0.6 GeV, and has a reduced $\bar{\nu}_e$ contamination and smaller backgrounds from higher energy neutrinos than the on-axis spectrum. Two detectors located 280 m from the target are used to measure the beam direction, spectrum, and composition, as well as the event rate: INGRID (on axis) [12], and ND280 (off axis), which is housed inside a 0.2 T magnet. The Super-Kamiokande (Super-K) 50-kt water Cherenkov detector [13], located off axis and 295 km from the neutrino production point, is used to detect oscillated neutrinos.

Data Sets — The results presented here are based on data collected in two periods: one in which the beam operated solely in neutrino mode, January 2010 — May 2013, and one in which the beam operated mostly in antineutrino mode, May 2014 — May 2016. This corresponds to a neutrino beam exposure of 7.482×10^{20} protons on target (POT) in neutrino mode and 7.471×10^{20} POT in antineutrino mode for the far detector analysis, and an exposure of 5.82×10^{20} POT in neutrino mode and 2.84×10^{20} POT in antineutrino mode for the near detector analysis.

Analysis Strategy — The analysis strategy is similar to that of previous T2K results [7, 9, 14, 15]: oscillation parameters are estimated by comparing predictions and observations at the far detector. A tuned prediction of the

oscillated spectrum at the far detector, with associated uncertainty, is obtained by fitting samples of charged-current interactions at ND280. The analysis presented here differs from previous results in that both neutrino and antineutrino samples are fitted at both ND280 and Super-K. Including antineutrino data at ND280 ensures that the interaction model is consistent between neutrinos and antineutrinos and provides a constraint on the wrong-sign background in the antineutrino-mode beam.

Neutrino Flux Model — The T2K neutrino and antineutrino fluxes at near and far detectors, and their correlations, are calculated [16] using a data-driven hybrid simulation with FLUKA 2011 [17, 18] used to simulate hadronic interactions and transport particles inside the target, while GEANT3 [19] with GCALOR [20] is used to simulate the rest of the neutrino beam line. The interactions of hadrons in both FLUKA 2011 and GCALOR are tuned using thin target hadron production data, including measurements of the total cross section for particle production, and π^\pm , K^\pm , p^\pm , Λ and K_S^0 production with 30 GeV protons on a graphite target by the NA61/SHINE experiment [21]. The uncertainty on the flux calculation is estimated by propagating systematic variations through the flux calculation procedure. Dominant systematic error sources include uncertainties on the NA61/SHINE hadron production measurements, hadronic interaction length measurements from NA61/SHINE and other experiments, the initial proton beam trajectory and the horn currents. The total uncertainty on the flux near the peak energy is $\sim 9\%$. The ν_μ ($\bar{\nu}_\mu$) component of the predicted fluxes without oscillations are shown in Fig. 1. At the far detector and in the absence of oscillations, we predict that 94.1% (92.3%) of the T2K neutrino-mode (antineutrino-mode) beam below 1.25 GeV is ν_μ ($\bar{\nu}_\mu$). The $\bar{\nu}_\mu$ flux in antineutrino mode is reduced by $\sim 20\%$ relative to the ν_μ flux in neutrino mode due to the smaller production cross section for π^- relative to π^+ in 30 GeV $p + C$ interactions.

Neutrino Interaction Model — The interactions of neutrinos and antineutrinos with nuclei in the near and far detectors are modelled with the NEUT [22] neutrino interaction generator. The charged-current quasielastic (CCQE) interactions are modelled with a relativistic Fermi gas (RFG) nuclear model with relativistic corrections for long range correlations using the random phase approximation (RPA) as applied by Nieves *et al.* [23]. The choice of CCQE nuclear model was made based on fits to external CCQE-like data [24] from the Mini-BooNE [25, 26] and MINERvA [27, 28] experiments. Interactions on more than one nucleon are modelled with an implementation of the 2p-2h model developed by Nieves *et al.* [29, 30]. These interactions are characterized by multi-nucleon ejection and no final state pions; hence they may be confused for CCQE interactions in a water Cherenkov detector. The single pion production model in NEUT has been tuned using form factors from Graczyk

and Sobczyk [31] and with a reanalysis of ANL and BNL bubble chamber data sets [32]. The coherent pion production model has been tuned to reproduce data from MINERvA [33] and T2K [34]. At the T2K peak energy, the antineutrino cross section is ~ 3.5 times smaller than the neutrino cross section.

The parameterization of uncertainties in the neutrino interaction model is largely unchanged from previous measurements [14, 15]. Parameters that vary the binding energy, Fermi momentum, 2p-2h normalization and charged current coherent cross-section normalization are applied separately for interactions on carbon and oxygen. To cover the different predictions by Nieves *et al.* [29, 30] and Martini *et al.* [35, 36] of the relative 2p-2h interaction rates for neutrinos and antineutrinos, the normalizations of 2p-2h interactions for neutrinos and antineutrinos are allowed to vary independently.

Only the interactions of ν_μ and $\bar{\nu}_\mu$ are explicitly constrained by near detector measurements in this analysis. Since the oscillation signals include ν_e and $\bar{\nu}_e$ interactions, it is necessary to assign uncertainties on the cross section ratios $\sigma_{\nu_e}/\sigma_{\nu_\mu}$ and $\sigma_{\bar{\nu}_e}/\sigma_{\bar{\nu}_\mu}$. Following the treatment in [37], separate parameters for $\sigma_{\nu_e}/\sigma_{\nu_\mu}$ and $\sigma_{\bar{\nu}_e}/\sigma_{\bar{\nu}_\mu}$ are introduced with a theoretical uncertainty of 2.8% for each. A correlation coefficient of -0.5 is assumed for these two parameters, accounting for anti-correlated changes to the relative cross section rates that can arise from nucleon form-factor variations.

Fit to Near Detector Data — The systematic parameters in the neutrino flux and interaction models are constrained by a fit to charged current (CC) candidate samples in the ND280 [10] near detector. The data sets used consist of reconstructed interactions in two fine-grained detectors (FGDs) [38] with particle tracking in three time projection chambers (TPCs) [39]. FGD2 contains six 2.54-cm-thick water panels, allowing systematic parameters governing neutrino interactions on H_2O , the same target as Super-K, to be directly constrained. The CC candidate samples in ND280 are divided into categories based on the beam mode (neutrino vs. antineutrino), the FGD in which the interaction takes place, the muon charge and the final state multiplicity. For data taken in neutrino mode, only interactions with a negatively charged muon are considered. For data taken in antineutrino mode, there are separate categories for events with positively-charged (right-sign) and negatively-charged (wrong-sign) muon candidates. The wrong-sign candidates are included because the larger neutrino cross section leads to a non-negligible wrong-sign background in antineutrino mode. In neutrino mode, there are three categories for reconstructed final states: no pion candidate in the final state (CC0 π), one pion candidate in the final state (CC1 π) and all other CC candidates (CC Other). In antineutrino mode, events are divided into two categories based on the final states: only the muon track exits the FGD to enter the TPC (CC

1-Track) and at least one other track enters the TPC (CC N-Track).

When fitting, the data are binned according to the momentum of the muon candidate, p_μ and $\cos\theta_\mu$, where θ_μ is the angle of the muon direction relative to the central axis of the detector, roughly 1.7° away from the incident (anti)neutrino direction. A binned maximum likelihood fit is performed in which the neutrino flux and interaction model parameters are allowed to vary. Nuisance parameters describing the systematic errors in the ND280 detector model – the largest of which is pion interaction modelling – are marginalised in the fit.

The fitted p_μ and $\cos\theta_\mu$ distributions for the FGD2 CC0 π and CC 1-Track categories are shown in Fig. 2. Acceptable agreement between the post-fit model and data is observed for both kinematic variables, with a p-value of 0.086. The best-fit fluxes are increased with respect to the original flux model by 10-15% near the flux peak. This is driven by the pre-fit deficit in the prediction for the CC0 π and CC Other samples. The fitted value for the axial mass in the CCQE model is $1.12 \text{ GeV}/c^2$, compared to $1.24 \text{ GeV}/c^2$ in a previous fit where the 2p-2h model and RPA corrections were not included [14]. The fit to ND280 data reduces the uncertainty on the event-rate predictions at the far detector due to uncertainties on the flux and ND280-constrained interaction model parameters from 10.9%(12.4%) to 2.9%(3.2%) for the ν_e ($\bar{\nu}_e$) candidate sample.

Far Detector Data — At the far detector, events are extracted that lie within $[-2, 10] \mu\text{s}$ relative to the beam arrival. Fully contained events within the fiducial volume are selected by requiring that no hit cluster is observed in the outer detector volume, that the distance from the reconstructed vertex to the inner detector wall is larger than 2 m, and that the total observed charge is greater than the equivalent quantity for a 30 MeV electron. The CCQE component of our sample is enhanced by selecting events with a single Cherenkov ring. The $\nu_\mu/\bar{\nu}_\mu$ CCQE candidate samples are then selected by requiring a μ -like ring using a PID-likelihood, zero or one decay electron candidates and muon momentum greater than 200 MeV/c to reduce pion background. Post selection, 135 and 66 events remain in the ν_μ and $\bar{\nu}_\mu$ candidate samples respectively, while if $|\Delta m_{32}^2| = 2.509 \times 10^{-3} \text{ eV}^2/c^4$ and $\sin^2 \theta_{23} = 0.528$ (i.e. maximal disappearance), 135.5 and 64.1 events are expected. The $\nu_e/\bar{\nu}_e$ CCQE candidate samples are selected by requiring an e-like ring, zero decay electron candidates, not π^0 -like and reconstructed energy less than 1.25 GeV. The total number of events remaining in these samples is presented in Table I with their respective expectation for different values of δ_{CP} , $\sin^2 2\theta_{13} = 0.085$, $|\Delta m_{32}^2| = 2.509 \times 10^{-3} \text{ eV}^2/c^4$, and $\sin^2 \theta_{23} = 0.528$. The ν_e ($\bar{\nu}_e$) contamination in the $\bar{\nu}_e$ (ν_e) sample is 17.4 (0.5) %, and the proportion of the sample expected to correspond to oscillated $\bar{\nu}_e$ (ν_e) events is 46.4 (80.9) % for $\delta_{CP} = -\pi/2$. A more detailed description

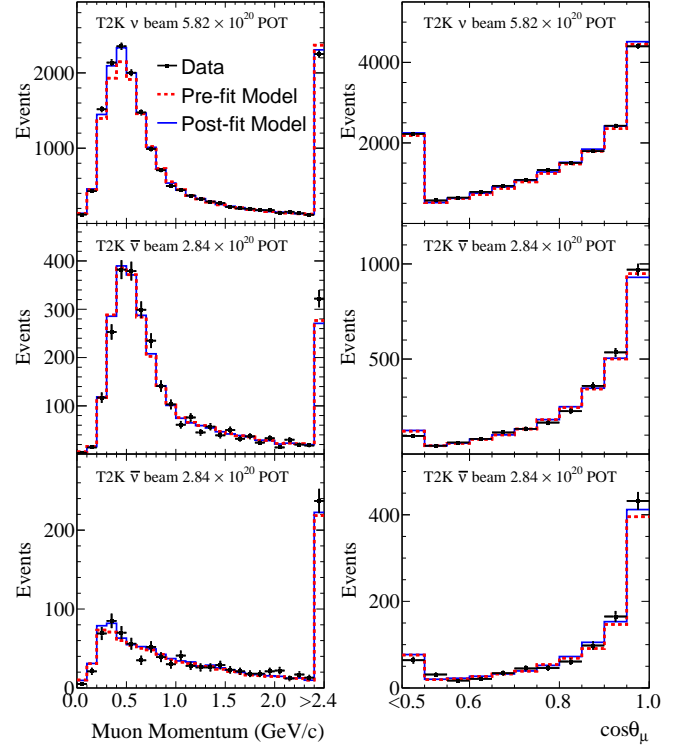


FIG. 2. The FGD2 data, pre-fit predictions and post-fit predictions binned in p_μ (left) and $\cos\theta_\mu$ (right) for the neutrino mode CC0 π (top), antineutrino mode CC 1-Track μ^+ (middle) and antineutrino mode CC 1-Track μ^- (bottom) categories. The overflow bins are integrated out to 10000 MeV/c and -1.0 for p_μ and the $\cos\theta_\mu$ respectively.

of the candidate event selections can be found in previous publications [14]. The reconstructed neutrino energy spectra for the ν_e and $\bar{\nu}_e$ samples is shown in Fig. 3. The $\bar{\nu}_e$ signal events are concentrated in the forward direction with respect to the beam, unlike the backgrounds. Therefore, incorporating reconstructed lepton angle information in the analysis increases the sensitivity.

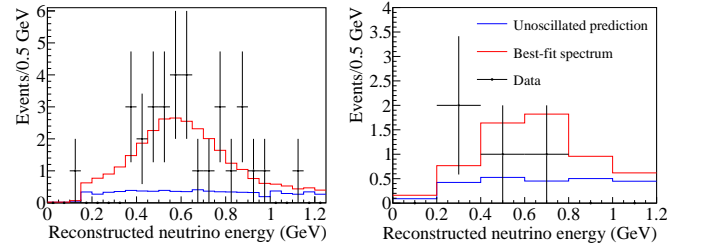


FIG. 3. The reconstructed neutrino energy at the far detector for the ν_e (left) and $\bar{\nu}_e$ (right) candidate samples is shown together with the expected distribution without oscillation (blue histogram) and the best fit (red histogram).

The systematic errors concerning the detector behaviour are estimated using atmospheric neutrino and

cosmic-ray muon events. A sample of hybrid data-MC events is also used to evaluate uncertainties regarding π^0 rejection. Correlations between the uncertainties for the four samples are considered.

TABLE I. Number of ν_e and $\bar{\nu}_e$ events expected for various values of δ_{CP} and both mass orderings compared to the observed numbers.

Normal	$\delta_{CP} = -\pi/2$	$\delta_{CP} = 0$	$\delta_{CP} = \pi/2$	$\delta_{CP} = \pi$	Observed
ν_e	28.7	24.2	19.6	24.1	32
$\bar{\nu}_e$	6.0	6.9	7.7	6.8	4
Inverted	$\delta_{CP} = -\pi/2$	$\delta_{CP} = 0$	$\delta_{CP} = \pi/2$	$\delta_{CP} = \pi$	Observed
ν_e	25.4	21.3	17.1	21.3	32
$\bar{\nu}_e$	6.5	7.4	8.4	7.4	4

The fractional variation of the number of expected events for the four samples owing to the various sources of systematic uncertainty are shown in Table II. A more in-depth description of the sources of systematic uncertainty in the fit is given in [14], although this reference does not cover the updates discussed in previous sections.

TABLE II. Systematic uncertainty on the predicted event rate at the far detector.

Source [%]	ν_μ	ν_e	$\bar{\nu}_\mu$	$\bar{\nu}_e$
ND280-unconstrained cross section	0.7	3.0	0.8	3.3
Flux and ND280-constrained cross section	2.8	2.9	3.3	3.2
SK detector systematics	3.9	2.4	3.3	3.1
Final or secondary hadron interactions	1.5	2.5	2.1	2.5
Total	5.0	5.4	5.2	6.2

Oscillation Analysis — The oscillation parameters $\sin^2 \theta_{23}$, Δm_{32}^2 , $\sin^2 \theta_{13}$ and δ_{CP} are estimated by performing a joint maximum-likelihood fit of the four far detector samples. The oscillation probabilities are calculated using the full three-flavor oscillation formulae [40]. Matter effects are included with an Earth density of $\rho = 2.6 \text{ g/cm}^3$ [41].

As described previously, the priors for the beam flux and neutrino interaction cross-section parameters are obtained from the fit with the near detector data. The priors [8] for the solar neutrino oscillation parameters – whose impact is almost negligible – are $\sin^2 2\theta_{12} = 0.846 \pm 0.021$, $\Delta m_{21}^2 = (7.53 \pm 0.18) \times 10^{-5} \text{ eV}^2/\text{c}^4$, and in some fits we use $\sin^2 2\theta_{13} = 0.085 \pm 0.005$ [8], called the “reactor measurement”. Flat priors are used for $\sin^2 \theta_{23}$, Δm_{32}^2 , and δ_{CP} .

We use a procedure analogous to [15]: after integrating over the prior distributions of the nuisance parameters a marginal likelihood, that depends only on the relevant oscillation parameters, is obtained. We define $-2\Delta \ln \mathcal{L} = -2\ln[\mathcal{L}(\mathbf{o})/\mathcal{L}_{max}]$ as the ratio between the marginal likelihood at the point \mathbf{o} of the relevant oscillation parameter space and the maximum marginal likeli-

hood.

We have conducted three analyses using different far detector event quantities and different statistical approaches. All of them use the neutrino energy reconstructed in the CCQE hypothesis (E_{rec}) for the $\bar{\nu}_\mu$ samples. The first analysis uses E_{rec} and the reconstructed angle between the lepton and the neutrino beam direction, θ_{lep} , of the $\bar{\nu}_e$ candidate samples and provides confidence intervals using a hybrid Bayesian-frequentist approach [42]. These results are shown in the following figures. The second analysis is fully Bayesian and uses the lepton momentum, p_{lep} , and θ_{lep} for the $\bar{\nu}_e$ samples to compute credible intervals using the posterior probability. The third analysis uses only E_{rec} spectra for the $\bar{\nu}_e$ samples and a Markov Chain Monte Carlo method [43] to provide Bayesian credible intervals. This analysis performs a simultaneous fit of both the near and far detector data, providing a validation of the extrapolation of the flux, cross section and detector systematic parameters from the near to far detector. All three methods are in good agreement.

An indication of the sensitivity to δ_{CP} and the mass ordering can be obtained from Table I. If CP violation is maximal ($\delta_{CP} = \pm\pi/2$), the predicted variation of the total number of events with respect to the CP conservation hypothesis ($\delta_{CP} = 0, \pi$) is about 20%. The different mass orderings induce a variation of the number of expected events of about 10%.

A series of fits are performed where one or two oscillation parameters are determined and the others are marginalised. Confidence regions are set using the constant $-2\Delta \ln L$ method [8]. In the first fit confidence regions in the $\sin^2 \theta_{23} - |\Delta m_{32}^2|$ plane (Fig. 4) were computed using the reactor measurement of $\sin^2 \theta_{13}$. The best-fit values are $\sin^2 \theta_{23} = 0.532$ and $|\Delta m_{32}^2| = 2.545 \times 10^{-3} \text{ eV}^2/\text{c}^4$ ($\sin^2 \theta_{23} = 0.534$ and $|\Delta m_{32}^2| = 2.510 \times 10^{-3} \text{ eV}^2/\text{c}^4$) for the normal (inverted) ordering. The result is consistent with maximal disappearance. The T2K data weakly prefer the second octant ($\sin^2 \theta_{23} > 0.5$) with a posterior probability of 61%.

Confidence regions in the $\sin^2 \theta_{13} - \delta_{CP}$ plane are computed independently for both mass ordering hypotheses (Fig. 5) without using the reactor measurement. The addition of antineutrino samples at Super-K gives the first sensitivity to δ_{CP} from T2K data alone. There is good agreement between the T2K result and the reactor measurement for $\sin^2 \theta_{13}$. For both mass-ordering hypotheses, the best-fit value of δ_{CP} is close to $-\pi/2$.

Confidence intervals for δ_{CP} are obtained using the Feldman-Cousins method [48]. The parameter $\sin^2 \theta_{13}$ is marginalised using the reactor measurement. The best-fit value is obtained for the normal ordering and $\delta_{CP} = -1.791$, close to maximal CP violation (Fig. 6). For inverted ordering the best-fit value of δ_{CP} is -1.414 . The hypothesis of CP conservation ($\delta_{CP} = 0, \pi$) is excluded at 90% C.L. and $\delta_{CP} = 0$ is excluded at more

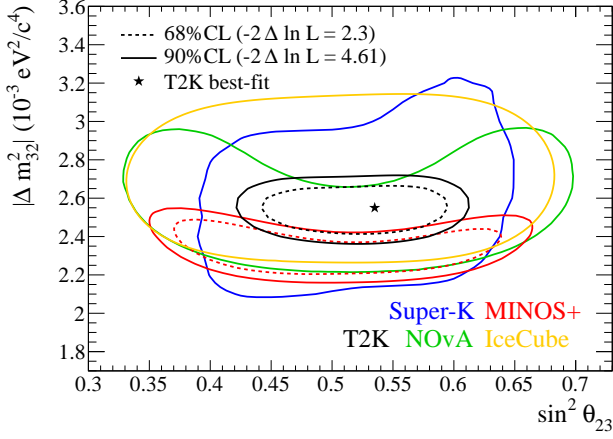


FIG. 4. The 68% (90%) constant $-2\Delta \ln L$ confidence regions for the $\sin^2 \theta_{23} - |\Delta m_{32}^2|$ plane assuming normal ordering, alongside NOvA[44], MINOS+[45], SK[46], and IceCube[47] confidence regions.

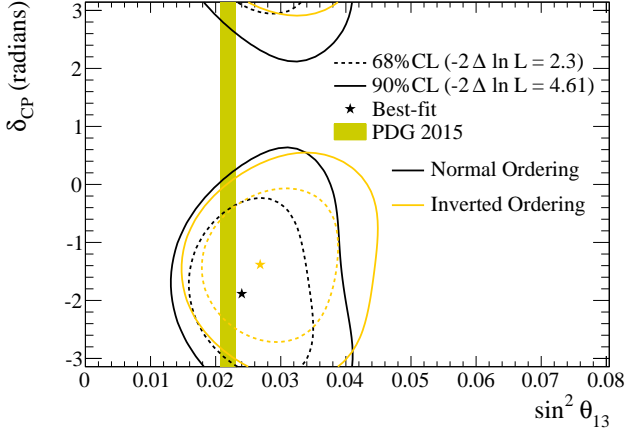


FIG. 5. The 68% (90%) constant $-2\Delta \ln L$ confidence regions in the $\delta_{CP} - \sin^2 \theta_{13}$ plane are shown by the dashed (continuous) lines, computed independently for the normal (black) and inverted (red) mass ordering. The best-fit point is shown by a star for each mass ordering hypothesis. The 68% confidence region from reactor experiments on $\sin^2 \theta_{13}$ is shown by the yellow vertical band.

than 2σ . The δ_{CP} confidence intervals at 90% C.L. are $(-3.13, -0.39)$ for normal ordering and $(-2.09, -0.74)$ for inverted ordering. The Bayesian credible interval at 90%, marginalising over the mass ordering, is $(-3.13, -0.21)$. The normal ordering is weakly favored over the inverted ordering with a posterior probability of 75%.

Sensitivity studies show that, if the true value of δ_{CP} is $-\pi/2$ and the mass ordering is normal, the fraction of pseudo-experiments where CP conservation ($\delta_{CP} = 0, \pi$) is excluded with a significance of 90% C.L. is 17.3%, with the amount of data used in this analysis.

Conclusions — T2K has performed the first search for

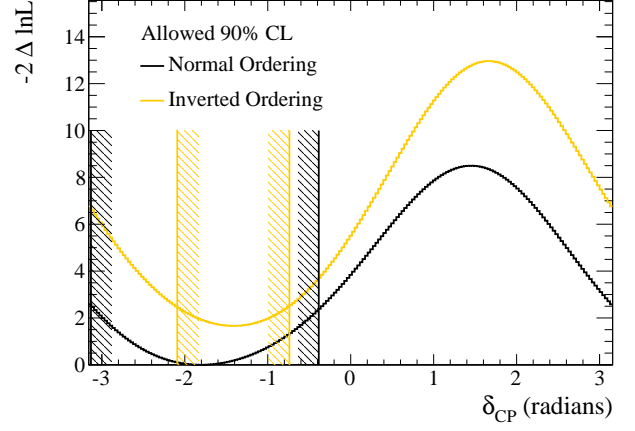


FIG. 6. $-2\Delta \ln \mathcal{L}$ as a function of δ_{CP} for the normal (black) and inverted (red) mass ordering. The vertical lines show the corresponding allowed 90% confidence intervals, calculated using the Feldman-Cousins method. $\sin^2 \theta_{13}$ is marginalised using the reactor measurement as prior probability.

CP violation in neutrino oscillations using $\nu_\mu \rightarrow \nu_e$ appearance and $\nu_\mu \rightarrow \nu_\mu$ disappearance channels in neutrino and antineutrino mode. The one-dimensional confidence interval at 90% for δ_{CP} spans the range $(-3.13, -0.39)$ in the normal mass ordering. The CP conservation hypothesis ($\delta_{CP} = 0, \pi$) is excluded at 90% C.L. The data related to the measurements and results presented in this Letter can be found in Reference[49].

We thank the J-PARC staff for the superb accelerator performance and the CERN NA61/SHINE collaboration for providing valuable particle production data. We acknowledge the support of MEXT, Japan; NSERC (grant SAPPJ-2014-00031), NRC and CFI, Canada; CEA and CNRS/IN2P3, France; DFG, Germany; INFN, Italy; National Science Centre (NCN), Poland; RSF, RFBR and MES, Russia; MINECO and ERDF funds, Spain; SNSF and SERI, Switzerland; STFC, UK; and DOE, USA. We also thank CERN for the UA1/NOMAD magnet, DESY for the HERA-B magnet mover system, NII for SINET4, the WestGrid and SciNet consortia in Compute Canada, and GridPP, UK. In addition, participation of individual researchers and institutions has been further supported by funds from: ERC (FP7), H2020 RISE-GA644294-JENNIFER, EU; JSPS, Japan; Royal Society, UK; DOE Early Career program, USA.

* also at J-PARC, Tokai, Japan

† affiliated member at Kavli IPMU (WPI), the University of Tokyo, Japan

‡ also at National Research Nuclear University "MEPhI" and Moscow Institute of Physics and Technology, Moscow, Russia

- [§] also at JINR, Dubna, Russia
[¶] also at Institute of Particle Physics, Canada
^{**} also at BMCC/CUNY, Science Department, New York, New York, U.S.A.
- [1] Z. Maki, M. Nakagawa, and S. Sakata, *Prog. Theor. Phys.* **28**, 870 (1962).
 - [2] B. Pontecorvo, *Sov. Phys. JETP* **26**, 984 (1968).
 - [3] K. Abe *et al.* (T2K), *Phys. Rev. Lett.* **107**, 041801 (2011).
 - [4] F. P. An *et al.*, *Phys. Rev. Lett.* **108**, 171803 (2012).
 - [5] J. K. Ahn *et al.*, *Phys. Rev. Lett.* **108**, 191802 (2012).
 - [6] Y. Abe *et al.* (Double Chooz Collaboration), *Phys. Rev. Lett.* **108**, 131801 (2012).
 - [7] K. Abe *et al.* (T2K Collaboration), *Phys. Rev. Lett.* **112**, 061802 (2014).
 - [8] K. A. Olive *et al.* (Particle Data Group), *Chin. Phys.* **C38**, 090001 ((2014) and 2015 update).
 - [9] K. Abe *et al.* (T2K Collaboration), *Phys. Rev. Lett.* **111**, 211803 (2013).
 - [10] K. Abe *et al.* (T2K Collaboration), *Nucl. Instrum. Methods* **A659**, 106 (2011).
 - [11] K. Suzuki *et al.* (T2K), *PTEP* **2015**, 053C01 (2015), arXiv:1412.0194 [physics.ins-det].
 - [12] K. Abe *et al.*, *Nucl. Instrum. Meth.* **A694**, 211 (2012), arXiv:1111.3119 [physics.ins-det].
 - [13] Y. Fukuda *et al.*, *Nucl. Instrum. Meth* **A501**, 418 (2003).
 - [14] K. Abe *et al.* (T2K Collaboration), *Phys. Rev.* **D91**, 072010 (2015).
 - [15] K. Abe *et al.* (T2K), *Phys. Rev. Lett.* **116**, 181801 (2016).
 - [16] K. Abe *et al.* (T2K Collaboration), *Phys. Rev.* **D87**, 012001 (2013), [Addendum: *Phys. Rev.D87*,no.1,019902(2013)].
 - [17] A. Ferrari, P. R. Sala, A. Fasso, and J. Ranft, Report No. CERN-2005-010 and SLAC-R-773 and INFN-TC-05-11 (2005).
 - [18] A. Ferrari, P. Sala, A. Fasso, and J. Ranft, *FLUKA: A Multi-Particle Transport Code* (2005).
 - [19] R. Brun, F. Bruyant, F. Carminati, S. Giani, M. Maire, A. McPherson, G. Patrick, and L. Urban, (1994).
 - [20] C. Zeitnitz and T. A. Gabriel, *Nucl. Instrum. Meth.* **A349**, 106 (1994).
 - [21] N. Abgrall *et al.* (NA61/SHINE Collaboration), *Eur. Phys. J.* **C76**, 84 (2016).
 - [22] Y. Hayato, *Acta Phys. Polon.* **B40**, 2477 (2009), version 5.3.2 of NEUT library is used that includes (i) the multinucleon ejection model of Nieves *et al.* [29] and (ii) nuclear long range correlations for CCQE interactions, treated in the random phase approximation [23].
 - [23] J. Nieves, J. E. Amaro, and M. Valverde, *Phys. Rev. C* **70**, 055503 (2004), [Erratum-ibid. *C* **72** (2005) 019902].
 - [24] C. Wilkinson *et al.*, *Phys. Rev. D* **93**, 072010 (2016).
 - [25] A. A. Aguilar-Arevalo *et al.* [MiniBooNE Collaboration], *Phys. Rev. D* **81**, 092005 (2010).
 - [26] A. A. Aguilar-Arevalo *et al.* (MiniBooNE), *Phys. Rev.* **D88**, 032001 (2013).
 - [27] G. Fiorentini *et al.* (MINERvA Collaboration), *Phys. Rev. Lett.* **111**, 022502 (2013).
 - [28] L. Fields *et al.* (MINERvA Collaboration), *Phys. Rev. Lett.* **111**, 022501 (2013).
 - [29] J. Nieves, I. Ruiz Simo, and M. J. Vicente Vacas, *Phys. Rev. C* **83**, 045501 (2011).
 - [30] R. Gran, J. Nieves, F. Sanchez, and M. J. Vicente Vacas, *Phys. Rev.* **D88**, 113007 (2013).
 - [31] K. M. Graczyk and J. T. Sobczyk, *Phys. Rev.* **D77**, 053001 (2008), [Erratum: *Phys. Rev.D79*,079903(2009)].
 - [32] C. Wilkinson, P. Rodrigues, S. Cartwright, L. Thompson, and K. McFarland, *Phys. Rev.* **D90**, 112017 (2014).
 - [33] A. Higuera *et al.* (MINERvA), *Phys. Rev. Lett.* **113**, 261802 (2014).
 - [34] K. Abe *et al.* (T2K), *Phys. Rev. Lett.* **117**, 192501 (2016).
 - [35] M. Martini, M. Ericson, G. Chanfray, and J. Marteau, *Phys. Rev.* **C80**, 065501 (2009).
 - [36] M. Martini and M. Ericson, *Phys. Rev.* **C87**, 065501 (2013).
 - [37] M. Day and K. S. McFarland, *Phys. Rev. D* **86**, 053003 (2012).
 - [38] P. Amaudruz *et al.* (T2K ND280 FGD Collaboration), *Nucl. Instrum. Methods* **A696**, 1 (2012).
 - [39] N. Abgrall *et al.* (T2K ND280 TPC Collaboration), *Nucl. Instrum. Methods* **A637**, 25 (2011).
 - [40] V. D. Barger, K. Whisnant, S. Pakvasa, and R. J. N. Phillips, *Phys. Rev.* **D22**, 2718 (1980).
 - [41] K. Hagiwara, N. Okamura, and K.-i. Senda, *J. High Energy Phys.* **09**, 082 (2011).
 - [42] R. D. Cousins and V. L. Highland, *Nucl. Instrum. Meth.* **A320**, 331 (1992).
 - [43] W. K. Hastings, *Biometrika* **57**, 97 (1970).
 - [44] P. Adamson *et al.* (NOvA), *Phys. Rev. D* **93**, 051104 (2016).
 - [45] P. Adamson *et al.*, *Phys. Rev. Lett.* **25**, 181801 (2013).
 - [46] R. Wendell, *Proc. of Science (ICRC 2015)*, 1062 (2015).
 - [47] M. Aartsen *et al.*, *Nucl. Phys.* **B908**, 161 (2016).
 - [48] G. J. Feldman and R. D. Cousins, *Phys. Rev.* **D57**, 3873 (1998).
 - [49] K. Abe *et al.* (T2K), <http://t2k-experiment.org/results/t2kdata-nu-antineutrino-joint-analysis-2016>.